Available online at website: https://journal.bcrec.id/index.php/bcrec

Bulletin of Chemical Reaction Engineering & Catalysis, 20 (2) 2025, 234-244

Original Research Article

One-pot Synthesis of MXene-derived Fe-N-C as Oxygen Reduction Reaction Catalyst in Acidic Medium

Norhamizah Hazirah Ahmad Junaidi[1], Wai Yin Wong[1]*, Kee Shyuan Loh[1], Thye Foo Choo[2], Jun Yu Wong[1], Li Wan Yoon[3]

[1]Fuel Cell Institute, Universiti Kebangsaan Malaysia, 43600 Bangi, Selangor, Malaysia
[2]Malaysian Nuclear Agency, Bangi, 43000 Kajang, Selangor, Malaysia
[3]Department of Engineering, School of Engineering and Technology, Sunway University, 47500 Bandar Sunway, Selangor, Malaysia.

Received: 9th November 2024; Revised: 12th March 2025; Accepted: 13th March 2025
Available online: 14th March 2025; Published regularly: August 2025

Abstract

Fe-N-C is a good candidate as the alternative to the expensive Pt/C catalyst for oxygen reduction reaction (ORR). However, its catalytic activity and durability are still inferior to the Pt/C catalyst. Recently, MXene has emerged as a promising material as the catalyst support for the ORR application due to its good conductivity and mechanical properties. In this work, the MXene-derived Fe-N-C catalyst was synthesized using the one-pot pyrolysis method, in which the MXene was directly added during the preparation of Fe-N-C at various pyrolysis temperatures and mass ratios of Fe salt. The works showed that the one-pot synthesis of Fe-N-C/MXene is ORR active, and has shown improved current density over Fe-N-C with the optimum pyrolysis temperature of 900 °C and mass ratio of 1:1. In addition, the Fe-N-C/MXene also demonstrated superior durability compared to Pt/C.

Keywords: Fe-N-C; MXene; One-pot synthesis method; Oxygen reduction reaction; Durability

How to Cite: Ahmad Junaidi, N. H., Wong, W. Y., Loh, K. S., Choo, T. F., Wong, J. Y., Yoon, L. W. (2025). One-pot Synthesis of MXene-derived Fe-N-C as Oxygen Reduction Reaction Catalyst in Acidic Medium. *Bulletin of Chemical Reaction Engineering & Catalysis*, 20 (2), 234-244. (doi: 10.9767/bcrec.20248)

Permalink/DOI: https://doi.org/10.9767/bcrec.20248

1. Introduction

Oxygen reduction reaction (ORR) is an important step in various electrochemical energy conversion devices, such as fuel cells and metal-air batteries [1]. In these devices, the ORR involves the reduction of oxygen molecules to water. Due to the sluggish reaction of ORR, an electrocatalyst is used to promote the reactions, thus increasing the efficiency of these energy conversion devices. Traditionally, Pt/C catalyst is used as the catalyst for ORR. However, the limited availability and the high cost of this material have led to research on alternatives to Pt-based catalysts.

Since a few years ago, Fe-N-C catalysts have emerged as promising candidates for ORR, offering a cost-effective and environmentally friendly alternative. The unique properties of Fe-N-C catalysts with their distinctive Fe-N_x moieties and nitrogen functional groups as the active sites make them suitable candidates for efficient and scalable electrocatalysts [2]. These active sites are commonly synthesized through the pyrolysis of nitrogen-rich metal complexes or a combination of metal salts, nitrogen and carbon-containing precursors [3]. However, the pyrolysis process causes a few challenges such as aggregation and the formation of thick catalyst layers, which could negatively impact mass transport. Therefore, catalyst support is required to overcome the issue of particle aggregation, thus improving their catalytic activity.

* Corresponding Author.
Email: waiyin.wong@ukm.edu.my (W. Y. Wong)

Since more than a decade ago, MXene has been introduced in many applications, such as batteries [4], supercapacitors [5], sensors [6] and many more including catalyst supports [7]. The exploration of MXenes in these applications is attributed to their excellent properties, especially their good conductivity and their strong mechanical properties [8]. MXenes can be synthesized at scale using green approaches such as physical based methods and HF-free synthesis to minimize the usage of toxic materials, thereby supporting a more sustainable and environmentally friendly fabrication process [9, 10]. Fe-N-C catalysts have been shown to exhibit high ORR activity, but they suffer from poor durability due to the leaching of active sites under harsh operating conditions [11]. Adding MXenes as a support can improve the stability and durability of the Fe-N-C catalyst. The addition of MXenes can enhance the catalytic activity of the Fe-N-C catalyst by improving the exposed active surface area, enhancing electron transfer and promoting the adsorption of reactant molecules [12]. Additionally, the MXenes can provide mechanical support to the Fe-N-C catalyst, reducing the aggregation of the active sites and preventing their detachment from the catalyst surface [13]. However, MXenes have an issue with their thermal stability. Despite their resistance to oxidation under normal conditions, MXenes are possible to experience oxidation at very high temperatures or prolonged exposure to oxidative environments [14]. This can lead to the degradation of the MXene structure. In our previous work, we attempted to introduce a two-pot synthesis method of MXene-support Fe-N-C [15]. The results have demonstrated improved ORR activity with significant improvement in the catalyst stability through the accelerated durability test (ADT). The work revealed that multilayer MXene can be effectively used as the Fe-N-C support which can avoid from the issue of restacking and oxidation of few layer MXene which is less stable.

While Fe-N-C catalysts derived from metal-organic frameworks (MOFs) have shown promising ORR activity, their synthesis often involves complex, multi-step processes that hinder scalability and practical application. In this work, we propose a novel one-pot synthesis method for MXene-derived Fe-N-C catalysts, which significantly simplifies the fabrication process compared to conventional two-step approaches. Unlike existing methods that require the separate formation of MOFs followed by their integration with MXene, our approach directly intercalates Fe-N-C active sites into the MXene structure, eliminating the need for pre-synthesized MOFs. This streamlined process not only reduces synthesis complexity but also induces potential morphological changes in the Fe-N-C structure, which may contribute to enhanced durability compared to traditional Pt/C catalysts. Therefore, this study aims to investigate the synthesis method of Fe-N-C/MXene as an oxygen reduction reaction catalyst in the acidic medium. This method involves the simultaneous formation of Fe-N-C species and MXene from a single precursor mixture. In this one-pot synthesis method, MXene is added with the same composition of mass as the iron precursor, followed by the different pyrolysis temperatures at the range of 800 to 1100 °C by considering the decomposition temperature of MXene and pyrolysis temperature of Fe-N-C as well as the evaporation of zinc ion. Further, the best temperature was selected as the pyrolysis temperature and subsequent experiments were carried out by varying the compositions of the Fe salt precursor and MXene with different mass ratios.

In general, higher Fe salt precursor content could lead to higher ORR activity due to the increased number of active sites for the ORR. However, if the Fe content is too high, it may lead to aggregation and loss of active sites [16], which would decrease the ORR activity. On the other hand, MXene serves as a support for the Fe-N-C catalyst and also contributes to the ORR activity through the synergistic effect between Fe-N-C and MXene. Therefore, the optimal ratio for achieving high ORR activity and stability can be determined by varying the mass ratio of Fe salt precursor and MXene. The specific ratios of 1:1, 4:1, 6:1, and 8:1 were chosen based on previous studies that indicated that these ratios could provide a range of Fe and MXene concentrations that are suitable for ORR catalysis [15,17]. Table 1 provides a comparative summary of various Fe-N-C based catalysts reported for ORR in acidic solution. Notably, studies on Fe-N-C/MXene catalyst in acidic media remain limited, as most studies focus on alkaline conditions. This gap further highlights the significance of this study which offers valuable insights into catalytic performance and durability of Fe-N-C/MXene for ORR in acidic environment, simulating the operating conditions of Proton Exchange Membrane Fuel Cells (PEMFCs).

2. Materials and Method

2.1 Synthesis of Fe-N-C/MXene

The one-pot synthesis of Fe-N-C/MXene was conducted by directly adding the multilayer $Ti_3C_2T_x$ (68%, ACS Materials) during the synthesis of Fe-N-C. In brief, 1.97 g of 2-methylimidazole (99%, Sigma Aldrich), 1.695 g of $Zn(NO_3)_2.6H_2O$ (R&M Chemicals) and 50 mg of $Fe(NO_3)_3.9H_2O$ (R&M Chemicals) were added into 600 ml of methanol solution (HmBG.) and stirred for 10 minutes. Next, 50 mg of $Ti_3C_2T_x$ MXene was added to obtain Fe-N-C/MXene with a mass ratio

of 1:1 (mass ratio of Fe salt to MXene). The solutions were stirred at 60 °C for 24 hours. The precipitate was then collected, washed using ethanol and dried at 60 °C in a vacuum oven overnight. After drying, the samples were collected, ground slowly using a pestle and mortar and pyrolyzed in a tube furnace with N_2 flow at a few different temperatures (T): 800 °C, 900 °C, 1000 °C and 1100 °C, for 1 hour (ramping rate of 5 °C min^{-1}). Finally, the samples were collected and labeled as Fe-N-C/MXene_1:1_T. Based on the optimum pyrolysis temperature tested for Fe-N-C/MXene_1:1_T samples, the pyrolysis temperature was selected to proceed with other mass ratios of 4:1, 6:1, and 8:1 by adjusting the amount of MXene based on prior studies. For comparison, Fe-N-C was prepared with the same procedure without the addition of MXene.

2.2 Physicochemical Characterizations

The morphology of the samples was characterized by using GeminiSEM 500 field emission scanning electron microscope and the crystallographic structure of the samples was characterized by using PANanalytical X'Pert PRO X-ray diffraction and analysed using Highscore Plus software. The chemical composition of the samples was investigated using Kratos Axis Ultra X-ray photoelectron spectroscopy (XPS) with Al Monochromatic. The surface area of the samples was determined using nitrogen adsorption-desorption analysis on Micromeritics Flex Analyser at 77K via Brunauer-Emmett-Teller (BET) method. The samples were degassed at 150 °C for 8 h to eliminate adsorbed gas or moisture on the surface before measurement.

2.3 Electrochemical Characterizations

The electrochemical characterization was conducted using a three-electrode cell on an Autolab PGSTAT128N potentiostat. The electrodes used include glass carbon working electrode, Ag/AgCl reference electrode and platinum counter electrode. The cyclic voltammetry (CV) test and the linear sweep voltammetry (LSV) test were conducted in 0.1 M $HClO_4$ electrolyte. The electrochemical tests were performed using the same method as our previous work [15]. Electron transfer number (n) and percentage of hydrogen peroxide (H_2O_2) produced were calculated using Equations (1) and (2), respectively [18], where I_d is the disk current, I_r is the ring current and N is the ring collection efficiency.

$$n = (4I_d)/(I_d + (I_r/N)) \quad (1)$$

$$H_2O_2(\%) = ((4 - n)/2) \times 100 \quad (2)$$

3. Results and Discussion

3.1 Effect of Pyrolysis Temperature

The effect of pyrolysis on the morphology of Fe-N-C/MXene catalysts with different pyrolysis temperatures is shown through FESEM characterization in Figure 1. From Figure 1, the Fe-N-C/MXene synthesized at different pyrolysis temperatures were seen deposited on the surface of the multilayer $Ti_3C_2T_x$ MXene. This is happening due to the direct addition of MXene in the salt precursors to synthesize the Fe-doped ZIF-8. In a standard procedure of synthesizing ZIF-8-derived Fe-N-C, high-temperature pyrolysis is needed for the formation of active

Table 1. Comparison of different Fe-N-C based samples on their ORR performance in 0.1 M $HClO_4$ from other studies.

Catalyst	E_{onset} (V vs. RHE)	Stability	Ref.
Fe-N-C	0.83	Almost 80% current is retained over 10000 s chronoamperometry test	This work
Fe-N-C/MXene_1:1_900	0.88	Retained 78.5% current over 10000 s chronoamperometry test; very small $E_{1/2}$ attenuation after 5000 ADT cycles	This work
Fe-N-C/$Ti_3C_2T_x$-(4:1)-500	0.88	Retained 94% current over 10000 s chronoamperometry test; only 7mV of $E_{1/2}$ decay after 5000 load cycles	[15]
Fe-N-C@MXene	-	11 mV $E_{1/2}$ attenuation after 10000 cyclic voltammetry cycles	[17]
Fe-N_x/N/Ti_3C_2	0.91	Almost 95% current retention after 10 hours	[29]
Fe-N-C-900	0.841	33mV of $E_{1/2}$ decay after 5000 load cycles	[30]
Pt/C	-	Maintained 61% current over 10000 s chronoamperometry test	[28]

sites. In addition, at this high temperature, Zn ions from the ZIF-8 precursor will evaporate, leaving behind the Fe-N-C with highly porous structure [15]. However, high-temperature pyrolysis is possible to damage the MXene surface. Therefore, lower pyrolysis temperature was investigated. From the FESEM image, it was observed that the lateral size of MXene decreased as the pyrolysis temperature increased. This phenomenon occurs, because the high temperature can cause the thermal degradation of the MXene sheets, resulting in the formation of smaller MXene sheets. In addition, high-temperature annealing can cause a reduction in the number of functional groups on the MXene sheets, which can lead to a decrease in interlayer spacing and sheet size [19].

During the heat treatment process, the organic linkers of ZIF-8 decomposed [20]. However, at lower temperatures such as 800 °C, the removal of Zn atoms from the material is not complete, leading to the detection of the Zn peak in the XRD pattern at 2θ = 43.1° (ICSD: 98-006-2860) as can be seen from the XRD pattern in Figure 2. As the pyrolysis temperature increases, the peaks at 43.1° slowly disappear and generate a sharp peak at 43.2° that corresponds to the (111) phase of Fe_3N (JCPDS No. 49-1664). In addition, when the pyrolysis temperature increases up to 1100 °C, it is observed that the 43.2° peaks become sharp and narrow, which indicates a more ordered crystal structure of Fe-N-C/MXene with an increased degree of crystallinity. At higher than 900 °C, distinct peak at 2θ = 27.3° and 54.3° were observed, indicating the formation of rutile TiO_2 with (110) and (211) crystal plane as according to the JCPDS #75-1537 [21,22]. This reveals that at a higher temperature, MXene starts to oxidize in the presence of oxidizing species to form TiO_2, which is also obtained by the findings from Han et al and Xu *et al.* [23,24]. Furthermore, at 800 °C, $Ti_3C_2T_x$ MXenes began to degrade and transform. According to Ji *et al.* [25], the degradation rate increased with the temperature, resulting in the transformation of $Ti_3C_2T_x$ MXenes into cubic TiC, as can be observed by the presence of the TiC peaks at 2θ = 36°, 40.2°, 72.6° and 76.4° (ICSD: 98-006-8281). Therefore, carefully selecting the pyrolysis temperature for the one-pot synthesis of Fe-N-C/MXene is crucial as high-temperature pyrolysis is important for the formation of the Fe-N_x active sites, while at the same time preventing the degradation of the MXene support.

The CV results from Figure 3 indicate that all Fe-N-C/MXene samples show a significant

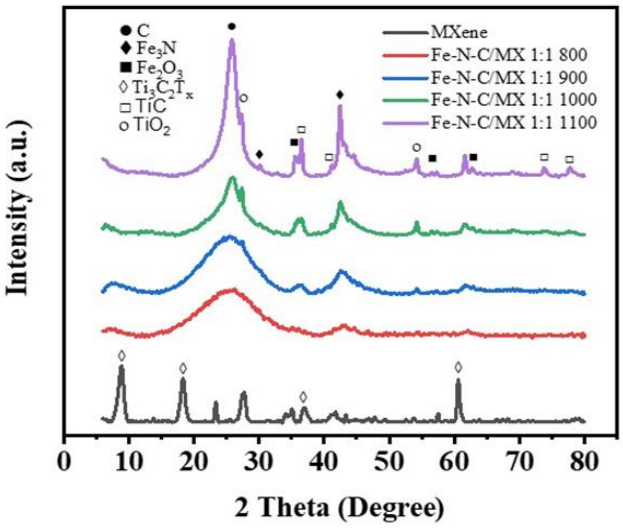

Figure 2. FESEM micrograph of pristine multilayer $Ti_3C_2T_x$ MXene and Fe-N-C/MXene synthesized with pyrolysis temperature of 800 °C, 900 °C, 1000 °C, and 1100 °C.

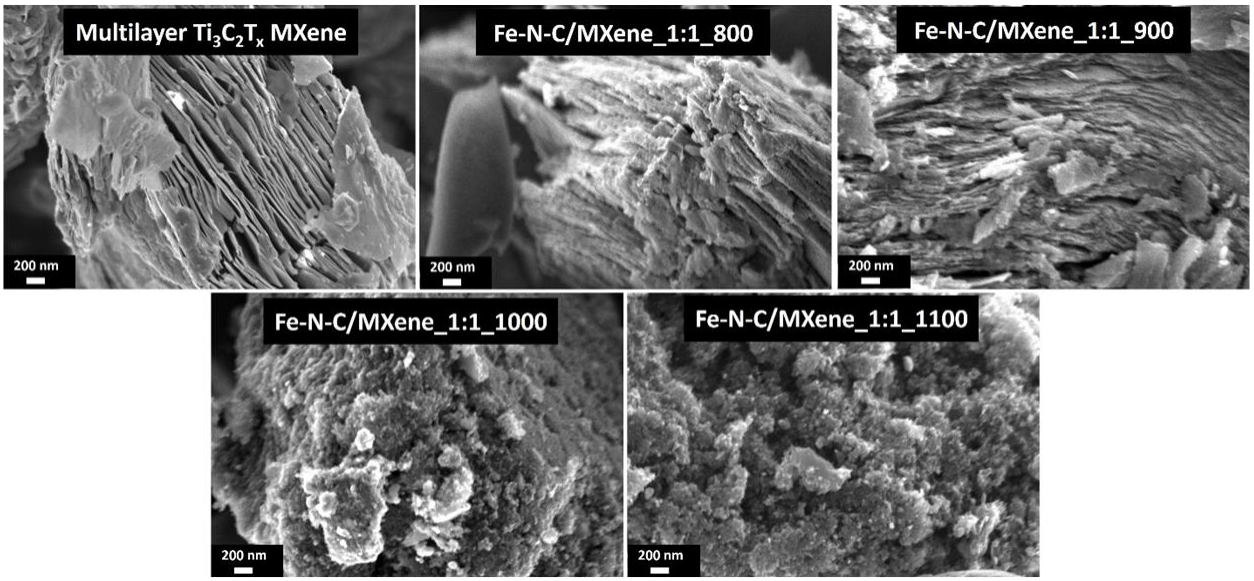

Figure 1. FESEM micrograph of pristine multilayer $Ti_3C_2T_x$ MXene and Fe-N-C/MXene synthesized with pyrolysis temperature of 800 °C, 900 °C, 1000 °C, and 1100 °C.

cathodic peak in an O_2-saturated electrolyte, suggesting the presence of ORR, except for the Fe-N-C/MXene_1:1 without pyrolysis. Figure 4 (a) shows the LSV curve of the Fe-N-C/MXene_1:1 catalyst. The Fe-N-C/MXene_1:1 without pyrolysis exhibits no catalytic activity due to the absence of active sites. This proves that high-temperature pyrolysis is necessary to form active sites for the ORR. All samples exhibited the onset potential (E_{onset}) within the range of 0.84 to 0.88 V vs. RHE. Interestingly, the Fe-N-C/MXene with the pyrolysis temperature of 900 °C shows a slight improvement compared to the Fe-N-C. In addition, the current density of the Fe-N-C/MXene_1:1_900 is the highest compared to the other Fe-N-C/MXene_1:1 and the Fe-N-C. According to Yu *et al.*, this can be attributed to the increased graphitization of the carbon matrix in the catalysts [26]. This correlates with the XRD result where the (002) planes of graphitic carbon peak shift to a more positive and become sharper as the pyrolysis temperature increases. However, when pyrolysis temperature exceeds 900 °C, excess graphitization with increased structural crystallinity leads to a decline in ORR performance. This is due to the higher graphitization reduces the density of defect site which are essential as active centers for ORR [27]. Additionally, at elevated temperature, MXene degradation leads to the formation of TiO_2 and TiC which are inherently inactive for ORR. The degradation further diminishes the availability of effective active site due to the loss of MXene layered structure [17]. Consequently, the combination effects of excess graphitization and MXene decomposition result in deterioration in catalytic activity. From the LSV, it can be concluded that the activity of the catalysts is in the descending order of Fe-N-C/MXene_1:1_900 > Fe-N-C > Fe-N-C/MXene_1:1_1000 > Fe-N-C/MXene_1:1_800 > Fe-N-C/MXene_1:1_1100.

From this set of experimental data, it can be concluded that the pyrolysis temperature at 900 °C is the optimum temperature as this temperature can partially remove the Zn ions from the ZIF-8 precursor and at the same time, forming the active site without further destroying the MXene support. From Figure 4 (b), the average electron transfer number of Fe-N-C/MXene_1:1_900 calculated using the rotating ring-disk electrode (RRDE) technique is 3.76, suggesting that this catalyst follows the 4-electron transfer for the ORR in acidic media. In addition, the percentage of H_2O_2 yield is less than 15 %, indicating low H_2O_2 produced during the reaction.

3.2 Effect of Mass Ratio

The amount of MXene support required for better performance is investigated by varying the mass ratio of the MXene added in the precursors. Figure 5 shows the FESEM micrograph of Fe-N-C/MXene with different MXene compositions at the pyrolysis temperature of 900 °C. When the mass ratio of the Fe salt precursor to MXene used is 1:1, the Fe-N-C particles are unifomly distributed on the surface of the MXene after pyrolysis. However, as the amount of Fe salt increases, it is observed that there are large particles on the MXene surface after pyrolysis. This could be due to the difficulty in evenly dispersing the larger number of Fe-N-C particles

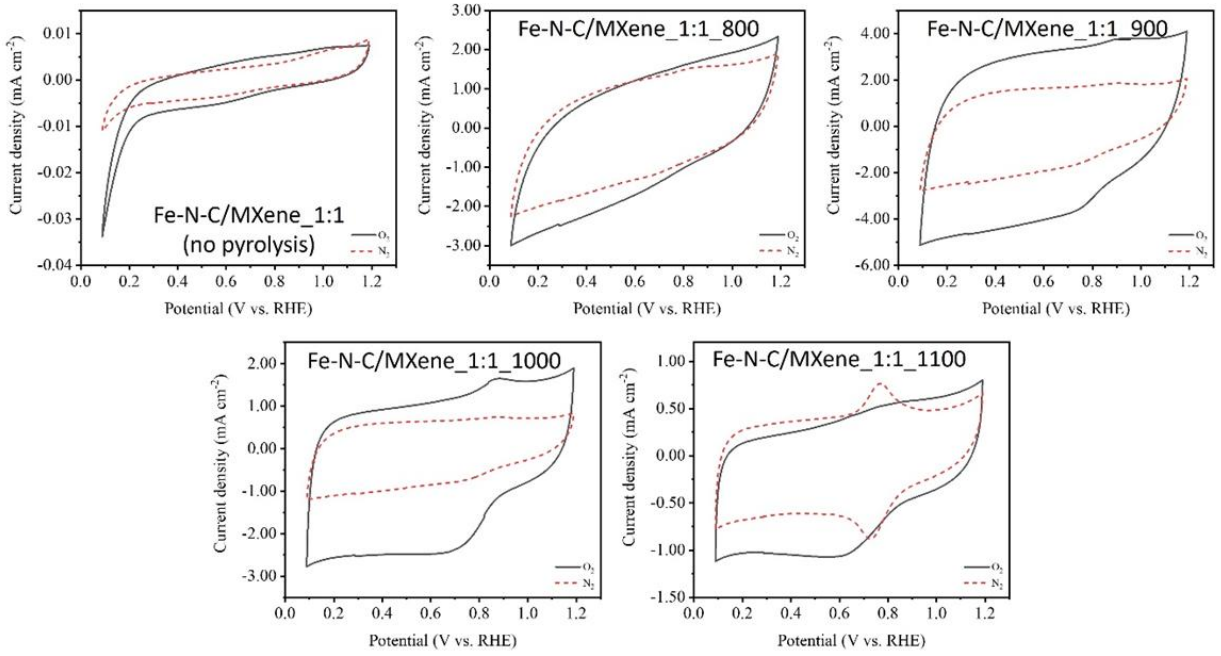

Figure 3. Cyclic voltammetry of Fe-N-C/MXene synthesized with no pyrolysis and pyrolysis temperature of 800 °C, 900 °C, 1000 °C, and 1100 °C.

on the MXene surface, leading to aggregation and the formation of large clusters. In addition, the higher concentration of Fe salt precursor could lead to increased agglomeration during the pyrolysis process, resulting in the formation of larger particles. This is because the addition of MXene can affect the growth of Fe-N-C with a hollow sphere structure during pyrolysis. The presence of MXene can provide a suitable template for the growth of Fe-N-C particles, leading to better dispersion and smaller particle size. On the other hand, MXene can also affect the chemical interactions and bonding between Fe-N-C and carbon during pyrolysis, changing in the final structure and properties of the synthesized material. Therefore, careful consideration of the Fe precursor to MXene ratio is important to achieve a well-dispersed and homogenous composite.

From the XRD pattern as shown in Figure 6 (a), an identical pattern was obtained for all Fe-N-C/MXene with different mass ratios pyrolyzed at the same pyrolysis temperature of 900 °C. Interestingly, it is found that the (002) plane of graphitic carbon at 2θ = 26° becomes narrower and sharpens as the amount of MXene added is reduced. From the LSV as shown in Figure 6 (b), the Fe-N-C/MXene_1:1_900 composition with a mass ratio of 1:1 exhibited the best catalytic activity with an E_{onset} of 0.88 V vs. RHE, which is higher than Fe-N-C alone (0.83 V vs. RHE). This suggests that the addition of MXene as a support

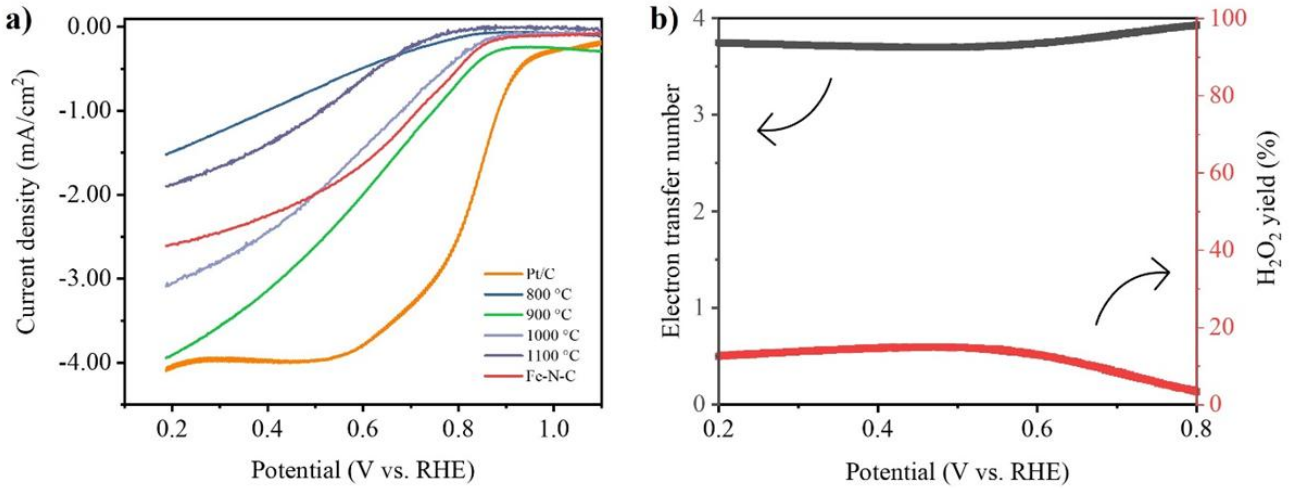

Figure 4. (a) Linear sweep voltammetry of Fe-N-C/MXene synthesized with different pyrolysis temperatures. (b) Electron transfer number and the percentage of H_2O_2 produced for Fe-N-C/MXene_1:1_900.

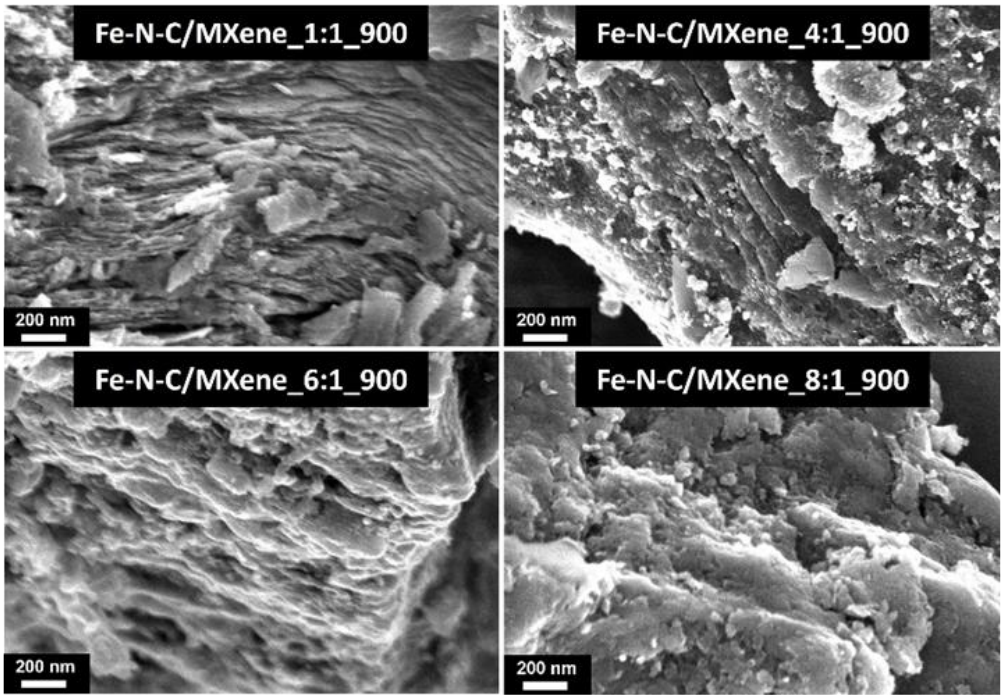

Figure 5. FESEM micrograph of Fe-N-C/MXene with different mass ratio pyrolyzed at 900 °C.

material enhances the electrocatalytic activity of Fe-N-C towards the ORR. Furthermore, the other Fe-N-C/MXene compositions exhibit the same E_{onset} of 0.87 V vs. RHE. This indicates that the amount of MXene added beyond a certain threshold does not significantly enhance the electrocatalytic activity of Fe-N-C for ORR. In addition, the current density of Fe-N-C/MXene_1:1_900 is also the highest, indicating that the electrocatalytic activity of this composition is better than the others, surpassing Fe-N-C prepared with the same method, as shown in Table 1. The higher current density can be attributed to the nature of MXene as a better electron conductor that can improve electron transfer during the oxygen reduction reaction, benefiting its use in many electrochemical applications such as fuel cells and batteries.

From the N_2 adsorption-desorption isotherm in Figure 6 (c), Fe-N-C/MXene_1:1_900 has an increased surface area (212.08 $m^2.g^{-1}$) compared to the pristine multilayer MXene (1.53 $m^2.g^{-1}$). The deconvoluted XPS N 1s spectra of Fe-N-C/MXene_1:1_900, as shown in Figure 6 (d) shows that there are TiN, pyridinic-N, Fe-N_x, pyrrolic N and graphitic-N bond that correspond to the binding energies at 397.2, 398.5, 399.4, 400.4 and 401.3 eV, respectively. The atomic composition of these bonding, compare to Fe-N-C, are tabulated in Table 2. It can be observed that the content of Fe-N_x in Fe-N-C/MXene_1:1_900 is significantly increased which is beneficial for ORR as Fe-N_x species act as highly active sites for the reaction. Additionally, graphitic-N and pyridinic-N dominated the configuration alongside Fe-N_x, playing an important role in stabilizing active

Table 2. Chemical composition of N 1s.

Atomic (%)	TiN	Pyridinic-N	Fe-N_x	Pyrrolic-N	Graphitic-N
Fe-N-C/MXene_1:1_900	13.4	21.02	24.31	11.91	29.37
Fe-N-C	-	3.60	8.98	33.04	54.38

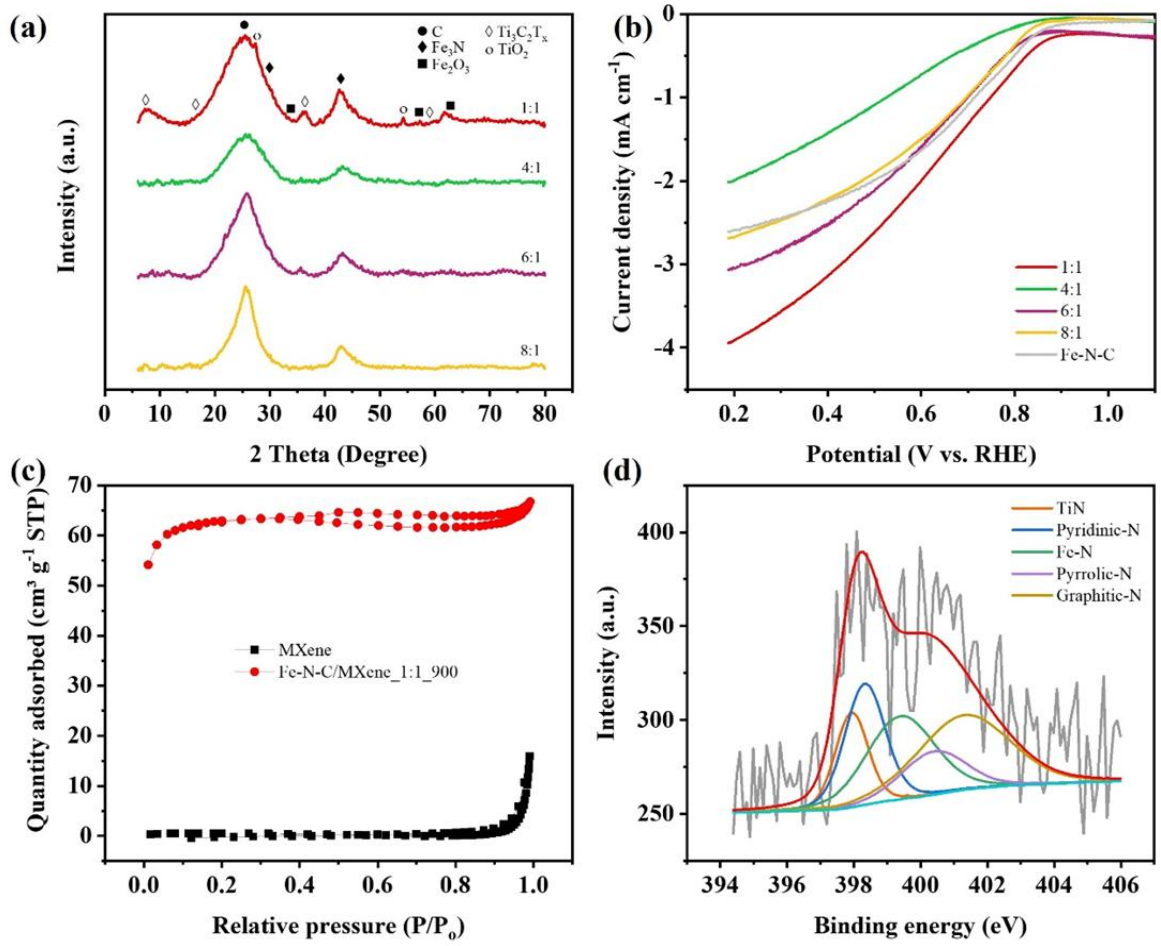

Figure 6. (a) XRD and (b) LSV of Fe-N-C/MXene with different mass ratio. (c) N2 adsorption-desorption isotherm of MXene and Fe-N-C/MXene_1:1_900. (d) The N1s spectra for Fe-N-C/MXene_1:1_900.

sites and reducing charge transfer resistance [17]. The intercalation of MXene into Fe-N-C structure induces synergistic effect with Fe-N_x, leading to the formation of Ti-N bonds. These Ti-N bonds not only modify the local electronic environment but also improve durability of the catalyst which agreed with previous study [15]. Although MXene may not directly participate in ORR, it significantly influences the overall catalytic activity. Its high electrical conductivity improves electron transport efficiency, facilitating fast charge transfer. The enhanced electron mobility not only increase the current density but also promotes the 4-electron ORR pathway to ensure complete reduction of oxygen. Overall, the addition of MXene as a support material in the Fe-N-C/MXene composite via the one-pot pyrolysis enhanced the ORR activity of Fe-N-C, and the optimal mass ratio for this composite is 1:1, reported in this work.

When compared with the two-pot synthesis method, this one-pot synthesis method shows a limitation on the suitable range of temperature that can be selected to create effective active sites on Fe-N-C [15]. In the presence of MXene during the synthesis of Fe-N-C from ZIF-8 precursor, the formation of a hollow structure of Fe-N-C could be inhibited [28]. Nonetheless, this work has unveiled the potential of the formation of ORR active sites with higher current density using the one-pot synthesis method, when compared to the Fe-N-C catalyst with hollow sphere structure. This further convinces the fact that MXene can form a strong bond with nitrogen in the Fe-N-C matrix (Ti-N), which helps alleviate the electron transfer through the conductive two-dimensional Ti_3C_2 layer.

Catalyst's durability is one of the factors that need to be considered. Therefore, the durability of the catalyst is tested using an accelerated durability test (ADT) with a load-cycle test protocol by applying the potential of 0.6 to 1.0 V vs. RHE. From Figure 7(b), the Fe-N-C/MXene_1:1_900 shows a very small attenuation in the $E_{1/2}$ compared to the commercial Pt/C (Figure 7(a)). In addition, the morphology of the Fe-N-C/MXene_1:1_900 shows only slight changes after the ADT (Figure 7(c)). This suggests that Fe-N-C is strongly anchored on MXene with no sign of active site deterioration under this load cycle potential range. This finding agrees with the two-pot synthesis method whereby Fe-N-C/MXene shows rather stable activity after the ADT [15]. Through the chronoamperometry test in O_2-

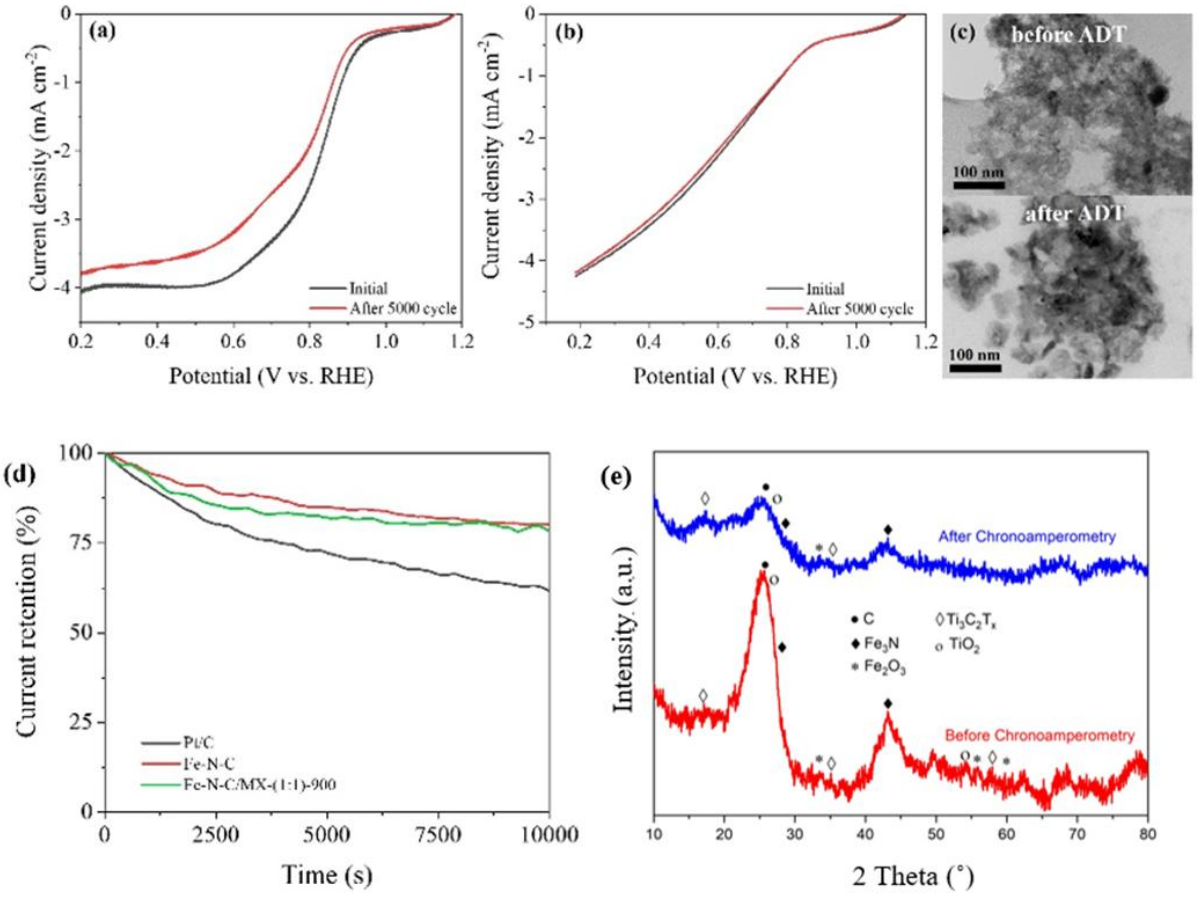

Figure 7. The LSV curve before and after the 5000 cycles ADT for (a) Pt/C and (b) Fe-N-C/MXene_1:1_900. The TEM image of Fe-N-C/MXene_1:1_900 (c) before and after the ADT. (d) Current-time chronoamperometry response for the Pt/C and Fe-N-C/MXene_1:1_900. (e) The XRD pattern before and after the chronoamperometry for Fe-N-C/MXene_1:1_900.

saturated 0.1 M $HClO_4$, as presented in Figure 7(d), Fe-N-C/MXene_1:1_900 could retain 78.5% of current over the 10000 s. Based on the XRD pattern (Figure 7 (e)), no phase change is observed in the Fe-N-C/MXene_1:1_900 sample deposited on glassy carbon after chronoamperometry. This indicates that the catalyst remains stable and durable under the operating conditions. Meanwhile, our previous work demonstrated that the current retention in the Fe-N-C/MXene with the two-pot synthesis method showed improvement over Fe-N-C catalyst [15]. Notably, the one-pot synthesis method has not shown a significant improvement over Fe-N-C catalyst. This can be attributed to the fewer active sites for ORR on the Fe-N-C catalyst as discussed earlier. More importantly, the stability of Fe-N-C/MXene_1:1_900 is still superior to the commercial Pt/C, though has lower current stability than Fe-N-C.

4. Conclusion

Based on the investigation, it can be concluded that the one-pot synthesis of Fe-N-C/MXene is ORR active and has shown improved current density over Fe-N-C. The best-performing sample is achieved at a mass ratio of 1:1 and a pyrolysis temperature of 900 °C. Increasing the amount of Fe salt used in the synthesis process may lead to decreased ORR activity due to the aggregation of Fe-N-C particles, which can block active sites. In terms of durability, Fe-N-C/MXene_1:1_900 still outperformed Pt/C with a current retention of 78.5% over 10000s. This highlights the one pot synthesis method incorporating MXene enhances the durability of the catalyst. However, its ORR performance remains implicitly lower than Pt/C, indicating the need for further optimization to enhance the catalytic activity due to the facile synthesis method. The future direction could focus on optimizing Fe-N-C/MXene by modifying the precursor of Fe-N-C to introduce more active sites, potentially improving catalytic activity. Upon further optimization, Fe-N-C/MXene can be tested in a complete fuel cell to access its real world-performance. Additionally, the high stability and improved current density of Fe-N-C/MXene could be explored for applications beyond ORR, including carbon dioxide reduction reaction (CO_2RR) and energy storage systems such as batteries. Furthermore, assessing the economic feasibility of the one-pot synthesis method through life cycle assessment (LCA) will provide valuable insights for large scale commercialization. These efforts will contribute to the development of more efficient and cost-effective catalyst for sustainable energy applications.

Acknowledgment

We would like to acknowledge the financial support of the Ministry of Higher Education (MOHE) Malaysia through the project of HiCoE SELFUEL (HICOE-2023-003).

CRediT Author Statement

Author Contributions: Norhamizah Hazirah Ahmad Junaidi: Writing - Original Draft; Methodology; Formal analysis; Data Curation; Wai Yin Wong: Conceptualization; Resources; Writing - Review & Editing; Project administration; Supervision; Funding acquisition; Kee Shyuan Loh: Writing - Review & Editing; Supervision; Thye Foo Choo: Investigation; Supervision; Jun Yu Wong: Investigation; Writing - Review & Editing; Li Wan Yoon: Writing - Review & Editing. All authors have read and agreed to the published version of the manuscript.

References

[1] Chai, L., Hu, Z., Wang, X., Zhang, L., Li, T.-T., Hu, Y., Pan, J., Qian, J., Huang, S. (2021). Fe7C3 nanoparticles with in situ grown CNT on nitrogen doped hollow carbon cube with greatly enhanced conductivity and ORR performance for alkaline fuel cell. *Carbon*. 174, 531-539. DOI: 10.1016/j.carbon.2020.12.070.

[2] Huang, Y., Liu, K., Kan, S., Liu, P., Hao, R., Liu, W., Wu, Y., Liu, H., Liu, M., Liu, K. (2021). Highly Dispersed Fe-N_x Active Sites on Graphitic-N Dominated Porous Carbon for Synergetic Catalysis of Oxygen Reduction Reaction. *Carbon*. 171, 1-9. DOI: 10.1016/j.carbon.2020.09.010.

[3] Jafari, M., Gharibi, H., Parnian, M.J., Nasrollahpour, M., Vafaee, M. (2021). Iron-Nanoparticle-Loaded Nitrogen-Doped Carbon Nanotube/Carbon Sheet Composites Derived from MOF as Electrocatalysts for an Oxygen Reduction Reaction. *ACS Applied Nano Materials*. 4 (1), 459-477. DOI: 10.1021/acsanm.0c02774.

[4] Dong, Y., Shi, H., Wu, Z.-S. (2020). Recent Advances and Promise of MXene-Based Nanostructures for High-Performance Metal Ion Batteries. *Advanced Functional Materials*. 30 (47), 2000706. DOI: 10.1002/adfm.202000706.

[5] Sohan, A., Banoth, P., Aleksandrova, M., Nirmala Grace, A., Kollu, P. (2021). Review on MXene synthesis, properties, and recent research exploring electrode architecture for supercapacitor applications. *International Journal of Energy Research*. 45 (14), 19746-19771. DOI: 10.1002/er.7068.

[6] Pei, Y., Zhang, X., Hui, Z., Zhou, J., Huang, X., Sun, G., Huang, W. (2021). Ti3C2TX MXene for Sensing Applications: Recent Progress, Design Principles, and Future Perspectives. *ACS Nano*. 15 (3), 3996-4017. DOI: 10.1021/acsnano.1c00248.

[7] Ahmad Junaidi, N.H., Wong, W.Y., Loh, K.S., Rahman, S., Daud, W.R.W. (2021). A Comprehensive Review of Mxenes as Catalyst Supports for the Oxygen Reduction Reaction in Fuel Cells. *International Journal of Energy Research*. 45 (11), 15760-15782. DOI: 10.1002/er.6899.

[8] Sinniah, J.D., Wong, W.Y., Loh, K.S., Yunus, R.M., Timmiati, S.N. (2022). Perspectives on Carbon-Alternative Materials as Pt Catalyst Supports for a Durable Oxygen Reduction Reaction in Proton Exchange Membrane Fuel Cells. *Journal of Power Sources*. 534, 231422. DOI: 10.1016/j.jpowsour.2022.231422.

[9] Shen, M., Jiang, W., Liang, K., Zhao, S., Tang, R., Zhang, L., Wang, J.Q. (2021). One-pot green process to synthesize MXene with controllable surface terminations using molten salts. *Angewandte Chemie*. 133 (52), 27219-27224. DOI: 10.1002/ange.202110640.

[10] Pang, S.-Y., Wong, Y.-T., Yuan, S., Liu, Y., Tsang, M.-K., Yang, Z., Huang, H., Wong, W.-T., Hao, J. (2019). Universal strategy for HF-free facile and rapid synthesis of two-dimensional MXenes as multifunctional energy materials. *Journal of the American Chemical Society*. 141 (24), 9610-9616. DOI: 10.1021/jacs.9b02578

[11] Peng, R., Zhao, Z., Sun, H., Yang, Y., Song, T., Yang, Y., Shao, J., Jin, H., Sun, H., Zhao, Z. (2023). The Active Sites and Corresponding Stability Challenges of the M-N-C Catalysts for Proton Exchange Membrane Fuel Cell. *Chinese Journal of Chemistry*. 41 (6), 710-724. DOI: 10.1002/cjoc.202200661.

[12] Jiang, L., Duan, J., Zhu, J., Chen, S., Antonietti, M. (2020). Iron-Cluster-Directed Synthesis of 2D/2D Fe-N-C/MXene Superlattice-like Heterostructure with Enhanced Oxygen Reduction Electrocatalysis. *ACS Nano*. 14 (2), 2436-2444. DOI: 10.1021/acsnano.9b09912.

[13] Wen, Y., Ma, C., Wei, Z., Zhu, X., Li, Z. (2019). FeNC/MXene hybrid nanosheet as an efficient electrocatalyst for oxygen reduction reaction. *RSC Advances*. 9 (24), 13424-13430. DOI: 10.1039/C9RA01330J

[14] Cao, F., Zhang, Y., Wang, H., Khan, K., Tareen, A.K., Qian, W., Zhang, H., Ågren, H. (2022). Recent advances in oxidation stable chemistry of 2D MXenes. *Advanced Materials*. 34 (13), 2107554. DOI: 10.1002/adma.202107554

[15] Ahmad Junaidi, N.H., Wong, W.Y., Loh, K.S., Rahman, S., Choo, T.F., Wu, B. (2023). Enhanced oxygen reduction reaction catalyst stability and durability of MXene-supported Fe-N-C catalyst for proton exchange membrane fuel cell application. *Journal of Alloys and Compounds*. 968 171898. DOI: 10.1016/j.jallcom.2023.171898.

[16] Zhang, H., Chung, H.T., Cullen, D.A., Wagner, S., Kramm, U.I., More, K.L., Zelenay, P., Wu, G. (2019). High-performance Fuel Cell Cathodes Exclusively Containing Atomically Dispersed Iron Active Sites. *Energy & Environmental Science*. 12 (8), 2548-2558. DOI: 10.1039/C9EE00877B.

[17] Wang, W.-T., Batool, N., Zhang, T.-H., Liu, J., Han, X.-F., Tian, J.-H., Yang, R. (2021). When MOFs meet MXenes: superior ORR performance in both alkaline and acidic solutions. *Journal of Materials Chemistry A*. 9 (7), 3952-3960. DOI: 10.1039/D0TA10811A

[18] Ao, X., Ding, Y., Nam, G., Soule, L., Jing, P., Zhao, B., Hwang, J.Y., Jang, J.-H., Wang, C., Liu, M. (2022). A Single-Atom Fe-N-C Catalyst with Ultrahigh Utilization of Active Sites for Efficient Oxygen Reduction. *Small*. 18 (30), 2203326. DOI: 10.1002/smll.202203326.

[19] Seredych, M., Shuck, C.E., Pinto, D., Alhabeb, M., Precetti, E., Deysher, G., Anasori, B., Kurra, N., Gogotsi, Y. (2019). High-Temperature Behavior and Surface Chemistry of Carbide MXenes Studied by Thermal Analysis. *Chemistry of Materials*. 31 (9), 3324-3332. DOI: 10.1021/acs.chemmater.9b00397.

[20] Zhang, H., Hwang, S., Wang, M., Feng, Z., Karakalos, S., Luo, L., Qiao, Z., Xie, X., Wang, C., Su, D., Shao, Y., Wu, G. (2017). Single Atomic Iron Catalysts for Oxygen Reduction in Acidic Media: Particle Size Control and Thermal Activation. *Journal of the American Chemical Society*. 139 (40), 14143-14149. DOI: 10.1021/jacs.7b06514.

[21] El-Desoky, M.M., Morad, I., Wasfy, M.H., Mansour, A.F. (2020). Synthesis, Structural and Electrical Properties of PVA/TiO_2 Nanocomposite Films with Different TiO_2 Phases Prepared by Sol–Gel Technique. *Journal of Materials Science: Materials in Electronics*. 31 (20), 17574-17584. DOI: 10.1007/s10854-020-04313-7.

[22] Moridon, S.N., Arifin, K., Mohamed, M.A., Minggu, L.J., Mohamad Yunus, R., Kassim, M.B. (2023). TiO2 Nanotubes Decorated with Mo2C for Enhanced Photoelectrochemical Water-Splitting Properties. *Materials*. 16 (18), DOI: 10.3390/ma16186261.

[23] Han, M., Yin, X., Wu, H., Hou, Z., Song, C., Li, X., Zhang, L., Cheng, L. (2016). Ti_3C_2 MXenes with Modified Surface for High-Performance Electromagnetic Absorption and Shielding in the X-Band. *ACS Applied Materials & Interfaces*. 8 (32), 21011-21019. DOI: 10.1021/acsami.6b06455.

[24] Xu, W., Li, S., Hu, S., Yu, W., Zhou, Y. (2021). Effect of Heat Treatment on Microwave Absorption Properties of $Ti_3C_2T_x$. *Journal of Materials Science: Materials in Electronics*. 32 (13), 17953-17965. DOI: 10.1007/s10854-021-06334-2.

[25] Ji, B., Fan, S., Ma, X., Hu, K., Wang, L., Luan, C., Deng, J., Cheng, L., Zhang, L. (2020). Electromagnetic Shielding Behavior of Heat-Treated $Ti_3C_2T_X$ MXene Accompanied by Structural and Phase Changes. *Carbon*. 165 150-162. DOI: 10.1016/j.carbon.2020.04.041.

[26] Yu, J., Jiang, Z., Huang, T., Tang, C. (2023). BN/Cu/CNT Nanoparticles as an Efficient Tri-Functional Electrocatalyst for ORR and OER. *International Journal of Hydrogen Energy*. 48, 53, 20368-20377. DOI: 10.1016/j.ijhydene.2023.03.015.

[27] Wassner, M., Eckardt, M., Reyer, A., Diemant, T., Elsaesser, M.S., Behm, R.J., Hüsing, N. (2020). Synthesis of amorphous and graphitized porous nitrogen-doped carbon spheres as oxygen reduction reaction catalysts. *Beilstein Journal of Nanotechnology*. 11 (1), 1-15. DOI: 10.3762/bjnano.11.1

[28] Ahmad Junaidi, N.H., Tan, S.Y., Wong, W.Y., Loh, K.S., Saidur, R., Choo, T.F., Wu, B. (2023). Influence of Fe–N–C morphologies on the oxygen reduction reaction in acidic and alkaline media. *Asia-Pacific Journal of Chemical Engineering*. 18 (6), e2950. DOI: 10.1002/apj.2950.

[29] Gu, W., Wu, M., Xu, J., Zhao, T. (2022). MXene boosted metal-organic framework-derived Fe–N–C as an efficient electrocatalyst for oxygen reduction reactions. *International Journal of Hydrogen Energy*. 47 (39), 17224-17232. DOI: 10.1016/j.ijhydene.2022.03.229.

[30] Li, Z., Liang, X., Gao, Q., Zhang, H., Xiao, H., Xu, P., Zhang, T., Liu, Z. (2019). Fe, N co-doped carbonaceous hollow spheres with self-grown carbon nanotubes as a high performance binary electrocatalyst. *Carbon*. 154 466-477. DOI: 10.1016/j.carbon.2019.08.036